¹⁸F-Fludarabine PET for Lymphoma Imaging: First-in-Humans Study on DLBCL and CLL Patients

Sylvain Chantepie*[1], Narinée Hovhannisyan*[2], Stéphane Guillouet[2], Jean-Pierre Pelage[3], Méziane Ibazizene[2], Caroline Bodet-Milin[4], Thomas Carlier[4], Anne-Claire Gac[1], Emilie Réboursière[1], Jean-Pierre Vilque[5], Françoise Kraeber-Bodéré[4], Alain Manrique[6], Gandhi Damaj[1,7,8], Michel Leporrier[2], and Louisa Barré[2]

[1]Hematology Institute, CHU de Caen, Caen, France; [2]CEA, CNRS, ISTCT/LDM-TEP Group, GIP Cyceron, Université de Caen Normandie, Caen, France; [3]Department of Radiology CHU de Caen, Caen, France; [4]Department of Nuclear Medicine, CHU de Nantes, Nantes, France; [5]Hematology Institute, Centre François Baclesse, Caen, France; [6]Department of Nuclear Medicine, CHU de Caen, Caen, France; [7]Microenvironnement et Cancers Hématologiques (MICAH), Université de Caen Normandie, Caen, France; and [8]INSERM U1245, Université de Rouen Normandie, Rouen, France

This was the first-in-humans clinical study of ¹⁸F-fludarabine, which is a radiopharmaceutical for PET imaging in lymphoma, for which many issues remain controversial with the standard radiotracer ¹⁸F-FDG. **Methods:** ¹⁸F-fludarabine PET or PET/CT was performed on 10 patients: 5 with diffuse large B-cell lymphoma (DLBCL) and 5 with chronic lymphocytic leukemia. The tumor uptake, biodistribution, and radiation dosimetry of ¹⁸F-fludarabine were evaluated. Six successive partial-body PET scans were acquired for 250 min after an intravenous 4 MBq/kg bolus of ¹⁸F-fludarabine. SUVs were recorded for each involved lymph node territory and for several extranodal sites, with particular reference to the liver. To assess the time-related uptake profile of ¹⁸F-fludarabine, PET images were analyzed by delineating volumes of interest over the uptake sites on the optimal scan for visual observation and were projected onto all coregistered scans of the same subject. Physical examination, laboratory studies, and contrast-enhanced CT were performed on all patients. For the DLBCL group, ¹⁸F-FDG PET was also considered. **Results:** In DLBCL patients, increased ¹⁸F-fludarabine uptake was observed in sites considered abnormal by CT or ¹⁸F-FDG, with SUVs significantly higher in involved lesions than in physiologic non-target sites. Nonetheless, the comparison of ¹⁸F-fludarabine and ¹⁸F-FDG PET showed discrepancies in 2 patients. In chronic lymphocytic leukemia patients, the uptake of ¹⁸F-fludarabine coincided with sites expected to be involved (including splenic invasion) according to conventional clinical and CT staging and was significant in hematopoietic bone marrow. No uptake was observed, whatever the disease group, in cardiac muscle or brain. The mean effective dose from an injected ¹⁸F-fludarabine activity of 305 ± 76 MBq was 3.07 ± 0.81 mSv. **Conclusion:** ¹⁸F-fludarabine PET might well be a promising tool for lymphoproliferative diseases. The radiation dose of this radiopharmaceutical is below that of ¹⁸F-FDG. The specificity of this PET probe for lymphoid cells, its absence of accumulation in reactive tissues, and its feasibility for detection of bone marrow infiltration might play an innovative role in lymphoma imaging.

Lymphomas are a diverse group of malignancies originating from lymphoid cells and are associated with variable prognosis. According to the different classification systems that have been applied over the years, including the recently updated REAL classification (Revised European-American Classification of Lymphoid Neoplasms), the 3 main categories of these lymphoid malignancies are Hodgkin lymphoma and non–Hodgkin lymphoma of B- or T-cell lineage (1). Although histologic confirmation is essential for the diagnosis, a reliable evaluation of the spread of lymphoma in vivo is possible only by imaging. The potential impact of molecular imaging by PET in oncology lies primarily in early tumor detection, evaluation of disease extent, and imaging-guided therapy evaluation (2–4). The most widely used PET tracer in lymphoma is ¹⁸F-FDG, which is clinically used for staging, therapy evaluation, and restaging (5,6). However, its uptake reflects the glycolytic activity of tissues, which is increased in most cancer cells. Although most malignant lymphomas such as Hodgkin lymphoma, diffuse large B-cell lymphoma (DLBCL), Burkitt cell lymphoma, mantle cell lymphoma, and follicular lymphoma are ¹⁸F-FDG–avid, with a PET/CT sensitivity of 85%–100% (7), ¹⁸F-FDG is not a highly tumor-specific tracer. Its uptake is also seen in activated macrophages and other inflammatory cells, leading to false-positive interpretations (8–10). Moreover, in some indolent non–Hodgkin lymphomas, including chronic lymphocytic leukemia, there is no established role for ¹⁸F-FDG PET because of the limited or variable avidity of ¹⁸F-FDG (11,12). In search of a more lymphoma-specific tracer, we have investigated and introduced ¹⁸F-fludarabine (13), an adenine nucleoside analog resistant to adenosine deaminase (14,15). Used alone or in association with other drugs (16,17), ¹⁸F-fludarabine demonstrates a significant antitumor efficacy in chronic lymphocytic leukemia (CLL) and indolent non–Hodgkin lymphoma. Interestingly, ¹⁸F-fludarabine has a special feature in that the base moiety has a fluorine atom, which can be replaced by ¹⁸F, a β-emitter, for

PET imaging. After developing radiochemistry suitable for enabling automated radiosynthesis (which includes delivering high yields, high reproducibility, and robustness, as well as provision of ^{18}F-fludarabine), we obtained preclinical PET data in vivo from different xenograft models of human lymphoma. Whereas ^{18}F-FDG accumulated in heart and brain, the ^{18}F-fludarabine radioactivity was considerably retained in tumor, providing a marked contrast between cancerous and healthy tissues (18). In a xenograft model, we demonstrated that ^{18}F-fludarabine was able to detect persistent viable lymphoid tissues during or after treatment (19). In a murine model of inflammation, we found that compared with ^{18}F-FDG, ^{18}F-fludarabine accumulated significantly less in the inflamed tissue (20). We assume that this tracer may allow differentiation between tumor mass and inflammation. Furthermore, because the cellular uptake of ^{18}F-fludarabine is cell-cycle–independent (21), ^{18}F-fludarabine PET/CT holds promise for imaging lymphoid neoplasms characterized by low mitotic activity. Therefore, to evaluate the potential role of ^{18}F-fludarabine in human lymphoma, we performed a pilot clinical study on 5 patients with newly diagnosed DLBCL and 5 patients with newly diagnosed CLL. For DLBCL patients, ^{18}F-FDG imaging was also conducted as recommended by the international guidelines. The study was also designed to determine the biodistribution and to estimate the absorbed radiation dose from ^{18}F-fludarabine in major organs.

MATERIALS AND METHODS

Patient Population

This prospective pilot clinical study was promoted by Caen University Hospital and conducted both at Cyceron Imaging Platform and at the Hematology Department of Caen University Hospital. To be eligible, patients had to be older than 18 y and have newly histologically confirmed DLBCL ($n = 5$) or previously untreated CLL ($n = 5$) requiring treatment according to the guidelines (22). DLBCLs were diagnosed by a reference pathologist on the basis of tissue samples according to the World Health Organization classification (23); CLL diagnosis was based on blood immunophenotype. The 10 patients were enrolled between May 20, 2014, and June 2, 2015. All patients gave written informed consent before study participation, according to the Declaration of Helsinki, and the protocol was approved by the responsible ethics committee (Comités de Protection des Personnes approval 2013-34). The study was registered at ClinicalTrials.gov (NCT02128945).

Physical examination, laboratory studies (blood counts, creatinine level, lactate dehydrogenase, and liver enzymes), and contrast-enhanced CT of the neck, chest, abdomen, and pelvis were performed on all patients. Safety was assessed by monitoring vital signs, laboratory test results, and adverse events. Patients were not eligible if they had an autoimmune hemolytic anemia, untreated infection, inadequate renal function with creatinine clearance lower than 30 mL/min, corticosteroid treatment, or any PET/CT contraindication.

Study Protocol and PET/CT Imaging

[18]F-fludarabine was produced with a radiochemical purity of more than 99% (13). ^{18}F-FDG was purchased from Cyclopharma Laboratories.

For all patients, ^{18}F-fludarabine scans were recorded on a Discovery RX VCT PET/CT system (GE Healthcare). PET and CT images were acquired in the same session, and both scans were obtained during normal tidal breathing. CT scans obtained with a low-dose protocol (80 kV, 50 mAs) were used for attenuation correction of the PET images. Six successive partial-body PET scans (from skull vertex to mid thigh) were acquired, with approximately 8 bed positions each, for 250 min after an intravenous 4 MBq/kg bolus of ^{18}F-fludarabine. Scanning times were 0–10, 15–25, 30–50, 90–100, 180–190, and 240–250 min after administration. The patients were repositioned with laser alignment between sequential scans. The average activity received by the patients was 305 ± 76 MBq (range, 217–444 MBq), with a ^{18}F-fludarabine mass of 0.23 ± 0.14 μg (range, 0.06–0.52 μg); the specific radioactivity was 450 ± 96 GBq/μmol. PET data were investigated using a 3-dimensional list-mode acquisition, and all appropriate corrections were applied for dead time, decay, random events, scatter, and attenuation. PET static images were reconstructed with the 3D VUE point HD algorithm (2 iterations, 9 subsets, and a filter of 3.43 mm in full width at half maximum; GE Healthcare) with a 128 × 128 matrix. Blood samples (5 mL) were collected at 60 and 240 min after administration, counted (Wizard 2470; PerkinElmer), and centrifuged at 1.21g for 15 min, and the radioactivity of the separated plasma was measured.

The DLBCL patients underwent, as part of routine clinical management, an initial staging by ^{18}F-FDG PET/CT at Caen University Hospital on a Biograph 6 TrueV-HD system (Siemens). The imaging session was performed 60–80 min after intravenous injection of 335 ± 77 MBq of ^{18}F-FDG. The mean interval between the ^{18}F-fludarabine and ^{18}F-FDG PET scans was 7 ± 2 d.

Image Analysis

To assess the time-related uptake profile of ^{18}F-fludarabine, PET images were analyzed by delineating volumes of interest over the uptake sites (as a general rule, on the 30- to 50-min scan) and projected onto all coregistered and decay-corrected scans of the same subject. For this purpose, the sequential CT scans of each patient were coregistered to the first CT scan of the study, and each PET scan was then matched to the corresponding CT scan. The SUV of the pixel with the highest uptake (SUV_{max}) was recorded in 10 nodal areas (region encompassing a single node or multiple nodes if present), including cervical, infraclavicular, axillary, mediastinal, hilar, paraaortic, mesenteric, inguinofemoral, iliac, and splenic, and in several extranodal regions: Waldeyer ring, liver, bone marrow, and muscle. SUV (based on body weight) was automatically calculated according to the classic formula. The ^{18}F-fludarabine PET scans were interpreted by 2 independent observers. PMOD 3.6 (PMOD Technologies, Ltd.) was used for data analysis. A masked centralized analysis of the ^{18}F-fludarabine PET images was performed using the Imagys platform (Keosys).

The metabolic tumor volume was defined as the volume of areas showing ^{18}F-fludarabine uptake. The segmentation of this volume was based on a background-level threshold (mean ± 2 × SD) (24), with liver considered background and an uptake-to-liver ratio of 1 or more considered the thresholding criterion (LIFEx, version 2.08; www.lifexsoft.org).

Because the PET cameras had not been cross-calibrated, no quantitative comparative analyses between the results for the 2 ^{18}F-labeled radiopharmaceuticals were performed. ^{18}F-FDG PET was interpreted visually using criteria recommended by the Lugano classification for lymphoma (25), and only positive foci were reported.

Dosimetry

Isocontour-based volumes of interest including the entire organs were defined (PMOD, version 3.6) on the sequential ^{18}F-fludarabine PET scan where the tissues were most visible (i.e., kidneys and liver on 0- to 10-min scan, spleen on 240- to 250-min scan). Lungs, brain, and heart wall volumes of interest were generated from aligned CT scans. Heart wall and heart blood pool could not be separated because contrast was insufficient. The defined volumes of interest were then projected onto all coregistered scans of the same subject. Organ volumes for each subject were assumed to be constant over time. The obtained time–activity curves were not decay-corrected, and a

biexponential fit was performed to integrate the time–activity curves. MIRD S factors were scaled to patient organ masses for dosimetric computation (26).

RESULTS

In all patients, the ^{18}F-fludarabine injections were well tolerated. One patient had a grade 2 liver enzyme elevation and grade 3 hyperbilirubinemia that were related to lymphoma. Orchidectomy was performed on 1 patient after the scan found lymphoma involvement. No significant modification of renal function and no cytopenias were observed after ^{18}F-fludarabine injection. The proportion of ^{18}F-fludarabine radioactivity in the plasma was higher in the DLBCL group than in the CLL group (Supplemental Fig. 1; supplemental materials are available at http://jnm.snmjournals.org).

DLBCL Patients

Histologic confirmation was obtained from the following sites: right cervical node (patient 2), right tonsil (patient 5), nasal cavity and right testis (patient 6), a mesenteric site (patient 8), and axillary node (patient 9). The disease was staged on a scale of I to IV based on the Lugano classification (Supplemental Table 1). Increased ^{18}F-fludarabine uptake was observed at sites considered abnormal on CT or ^{18}F-FDG images, including nodal sites (e.g., cervical, axillary, mediastinal, or paraaortic) and extranodal sites (e.g., spleen or bone marrow). For suspected abnormal lesions in which uptake was higher than in liver, SUV$_{max}$ is reported in Supplemental Table 2. In all patients, SUVs were significantly higher in involved lesions than in physiologic nontarget sites (Supplemental Table 2; Fig. 1). The average ^{18}F-fludarabine PET SUV$_{max}$ for the involved sites was 7.14 (range, 5.24–9.10) at the 30- to 50-min scan and 10.16 (range, 4.54–14.31) at the 240- to 250-min last scan. Uptake of ^{18}F-fludarabine at 30–50 min after injection remained higher in tumor than in ascending aorta (SUV$_{max}$, 1.42; range, 1.32–1.51), muscle (SUV$_{max}$, 1.29; range, 1.13–1.45), or liver (SUV$_{max}$, 2.58; range, 2.21–3.08). Progressive clearance of radioactivity was observed from blood pool and muscle, whereas uptake was slightly enhanced (1.3 times) in liver on the last scan. In all cases, bone marrow was histologically normal (Supplemental Table 1) and no hyperactivity was observed on the 30- to 50-min early ^{18}F-fludarabine PET scan (SUV$_{max}$, 2.33; range, 2.17–2.54);
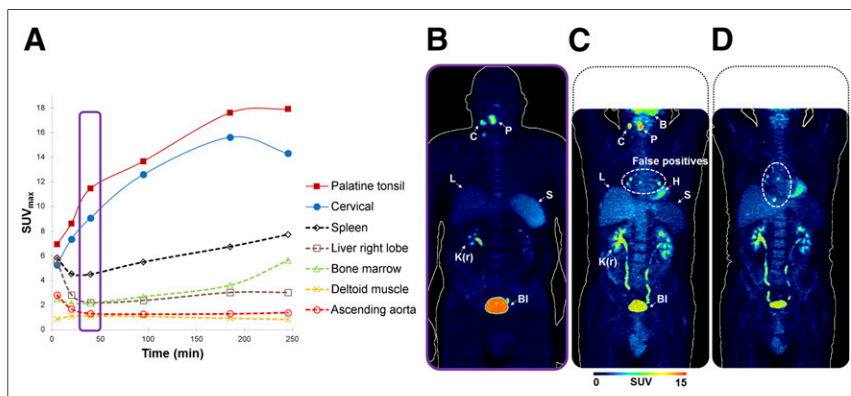
nevertheless, on the 240- to 250-min last scan the uptake was increased nearly 2-fold, slightly exceeding the liver uptake (1.3 times, Supplemental Fig. 2). Progressive splenic uptake was observed in all patients, with an average SUV$_{max}$ of 4.91 (range, 3.46–5.94) at 50 min after injection to 7.71 (range, 4.81–9.83) at 250 min.

^{18}F-FDG PET and ^{18}F-fludarabine PET showed interesting discrepancies in some cases, with the 2 most significant ones as follows: patient 5 showed mediastinal lymph node uptake with ^{18}F-FDG (Fig. 1C) but not with ^{18}F-fludarabine (Fig. 1B). The ^{18}F-FDG uptake persisted after completion of the treatment and disappearance of all suspected pathologic sites (Fig. 1D). The patient was considered in complete remission and remained relapse-free at more than 2 y after completion of the chemotherapy. Patient 6 had an ^{18}F-FDG–positive right testis, whereas the ^{18}F-fludarabine findings were considered negative, with uptake close to the background level. Orchidectomy was performed, and lymphomatous involvement of the testis was confirmed histologically.

CLL Patients

In the 5 CLL patients, the major ^{18}F-fludarabine accumulation coincided with sites expected to be involved according to conventional clinical and CT scan staging (i.e., lymph nodes and spleen) (Supplemental Tables 3 and 4). For instance, the most active sites were lymph nodes, with the average ^{18}F-fludarabine PET SUV$_{max}$ being 6.05 (range, 4.82–7.42) on the 30- to 50-min scan and 10.30 (range, 6.96–12.22) on the last scan.

An important and progressive splenic uptake (Figs. 2 and 3), more elevated than in DLBCL group, was detected in all CLL subjects, with an average SUV$_{max}$ of 7.73 (range, 6.35–9.88) at 50 min after injection and 12.39 (range, 10.46–16.41) at 250 min. Bone marrow infiltration was detected by elevated retention of the radiopharmaceutical at 30–50 min after injection (SUV$_{max}$, 4.37; range, 3.59–5.40) in comparison with the radioactivity in ascending aorta (SUV$_{max}$, 1.52; range, 1.27–1.73), muscle (SUV$_{max}$, 1.32; range, 1.05–1.47), and liver as background level (SUV$_{max}$, 2.59; range, 2.50–2.66). Continuous accumulation in bone marrow over the 250-min acquisition was evident in all patients (SUV$_{max}$, 7.62; range, 6.70–8.86). Progressive clearance of radioactivity was observed from blood and muscle, whereas uptake was slightly enhanced (1.4 times) in liver at the last scan.
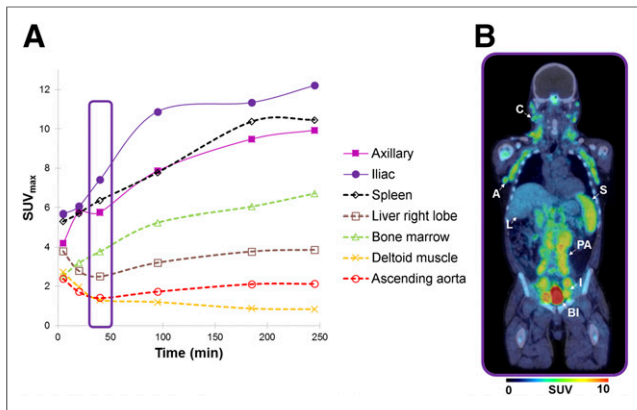
Other Observations

In 6 of 8 patients (not applicable for the other 2 patients), ^{18}F-fludarabine PET showed similar retention in an anatomic zone that could correspond to Peyer patches, visible only on the later scans (>180 min after injection), with an average SUV$_{max}$ of 1.85 on the 30- to 50-min scan and 6.17 (range, 3.38–7.7) on the 240-to- 250-min scan.

Regarding the tonsils, most patients showed a mild degree of ^{18}F-fludarabine incorporation. The exception was 1 DLBCL patient (patient 5), who had high ^{18}F-fludarabine uptake in the right palatine tonsil (SUV$_{max}$, 11.46 at 30–50 min and 17.92 at 240–250 min) in accordance with the biopsy result (Supplemental Table 1). In patient 6, a paranasal sinus involvement was detected, with an elevated SUV$_{max}$ of 7.87 at 30–50 min increasing to 10.7 at 240–250 min;

FIGURE 1. Representative DLBCL patient (patient 5). (A) Time–activity curves of ^{18}F-fludarabine after intravenous injection (4 MBq/kg). (B–D) Maximum-intensity projections of typical ^{18}F-fludarabine PET scan (30–50 min, scan period surrounded by border on chart) (B), ^{18}F-FDG PET scan (60–80 min) (C), and posttreatment ^{18}F-FDG PET scan (60–80 min) (D) of same patient, displayed using same color scale. B = brain; Bl = bladder; C = cervical node; H = heart; K(r) = right kidney; L = liver; P = palatine tonsil; S = spleen.

FIGURE 2. Representative CLL patient (patient 3). (A) Time–activity curves of ^{18}F-fludarabine after intravenous injection (4 MBq/kg). (B) Maximum-intensity projection of ^{18}F-fludarabine PET/CT scan (30–50 min, scan period surrounded by border on chart). A = axillary nodes; Bl = bladder; C = cervical nodes; I = iliac nodes; L = liver; PA = paraaortic nodes; S = spleen.

by comparison, in 2 CLL patients (patients 4 and 7) the variation in SUV_{max} was less pronounced and the values lower (3.7 at 30–50 min and 4.9 at 240–250 min).

As reported in Supplemental Tables 2 and 4, the involved sites were already detectable at 30–50 min, with marked contrast between tumoral and normal tissues. Furthermore, in agreement with former preclinical studies (18), no uptake was observed in cardiac muscle or brain. The metabolic tumor volume was 158 cm^3 for the DLBCL group (range, 100–221 cm^3) and 2,376 cm^3 for the CLL group (range, 421–3,664 cm^3; most of this volume included active medullar [19%] and splenic [47%] tissues) as assessed on the 30- to 50-min scan.

The estimated organ doses and the effective dose for each group are shown in Supplemental Table 5. The mean effective dose per unit activity administered was 0.008 ± 0.001 mSv/MBq for DLBCL ($n = 4$) and 0.013 ± 0.002 mSv/MBq for CLL ($n = 4$). In both groups, the spleen was the organ with the highest radiation burden (0.023 ± 0.007 mGy/MBq for DLBCL; 0.052 ± 0.031 mGy/MBq for CLL). The highest coefficient of variance (58.92%, for CLL) was obtained for spleen, possibly because of the various degrees of splenic involvement across subjects.

DISCUSSION

The present study involved the first-in-humans administration of ^{18}F-fludarabine. The development of this PET probe was based on the characteristics of ^{18}F-fludarabine, a drug that has a high level of activity against a variety of indolent lymphoproliferative malignancies, including CLL and low-grade non-Hodgkin lymphoma (14,15). The aim of this study was to evaluate the accuracy of ^{18}F-fludarabine PET/CT in diagnosing DLBCL and CLL, which have different affinities for ^{18}F-FDG. Although PET based on ^{18}F-FDG is relevant in the diagnosis, staging, and therapy monitoring of lymphoma (25), the interpretation of ^{18}F-FDG–avid lymphomas is sometimes questioned, mainly because of the lack of specificity of ^{18}F-FDG. In several preclinical investigations, we highlighted the great potential of ^{18}F-fludarabine PET for accurate imaging of lymphoproliferative disorders (18,19). As previously demonstrated (20), uptake of this PET probe is inflammation-independent—a crucial characteristic for identifying tumor burden during chemotherapy or radiotherapy, both of which are a source of inflammatory processes that can be responsible for false-positive ^{18}F-FDG PET results.

In this human study investigating 2 types of hematologic malignancy, all ^{18}F-fludarabine injections were well tolerated and had no adverse effects. Of note, and as previously described for preclinical studies, ^{18}F-fludarabine did not show brain or heart uptake. This low background uptake may facilitate detection of mediastinal and hilar foci and enable identification of central nervous system lymphoma when the blood–brain barrier has been disrupted.

In DLBCL, ^{18}F-fludarabine uptake was significantly concordant with ^{18}F-FDG–positive sites. Nevertheless, the result in patient 5 (Fig. 1; Supplemental Table 2), who showed nonspecific ^{18}F-FDG uptake in mediastinal lymph nodes (e.g., probable granulomatosis) and no uptake of ^{18}F-fludarabine, suggests that ^{18}F-fludarabine is more specific than ^{18}F-FDG—the patient remaining relapse-free at more than 2 y after completion of the chemotherapy. Indeed, it is known that false-positive ^{18}F-FDG PET results occur in a considerable proportion of treated DLBCL patients (10,27). Moreover, as recently reported (28), it is quite impossible to characterize mediastinal lymphadenopathy as benign (e.g., as tuberculosis or sarcoidosis) or malignant on the basis of ^{18}F-FDG or ^{18}F-FLT PET, even though they reflect different aspects of biology (i.e., metabolism and proliferation, respectively). The potential capacity of ^{18}F-fludarabine to distinguish tumor burden from inflammatory tissue is also crucial for predicting viable lymphoma in residual masses after completion of therapy. On the other hand, ^{18}F-fludarabine PET did not detect the lymphomatous infiltration in the testis of patient 6, a classic extranodal site for lymphoma; the role of the testis barrier might explain that issue (29).

In CLL, ^{18}F-fludarabine PET showed uptake in all sites that had been suspected on the basis of the CT results. Nevertheless, additional patterns of ^{18}F-fludarabine activity were observed in nodal sites (mediastinal and hilar in patient 7, paraaortic and mesenteric in patient 10) and extranodal sites (skull in patient 10, nasal in patient 4, bone marrow in all CLL patients) (Supplemental Table 4); histologic confirmation of the CLL localization in these additional sites was not specifically obtained. Indeed, functional imaging with ^{18}F-fludarabine PET may be a real tool for CLL diagnosis, enabling the imaging of bone marrow involvement as an index of CLL disease. Furthermore, whereas splenomegaly was not identified in patient 7, the SUV_{max} of ^{18}F-fludarabine in the spleen was comparable to that in other patients, suggesting a specific splenic infiltration.

Considering all enrolled patients, the 2 groups showed a trend toward differential responses (Fig. 3). ^{18}F-fludarabine uptake by lymphoma lesions in extranodal sites (bone marrow and spleen) was higher for CLL patients than for DLBCL patients. Within the involved nodes and the nontarget tissues, the 2 groups had overlapping uptake profiles. Some nodal localizations demonstrated a continued slow uptake throughout the 250 min, and others showed a relative plateau on the later scans. Although the greatest difference between tumor and physiologic tissues appeared on the later ^{18}F-fludarabine PET scans, good differentiation was also notable earlier (Figs. 1 and 2; Supplemental Fig. 2). In addition, ^{18}F-fludarabine demonstrated a wide range of uptake that would indicate heterogeneity of disease activity within differing microenvironments. Furthermore, most DLBCL patients had unilateral involvement, whereas CLL patients had a high frequency of bilateral involvement, with a significantly larger metabolic tumor volume than in the DLBCL group. Metabolic tumor volume may be a relevant parameter for disease monitoring (30,31). In this study,
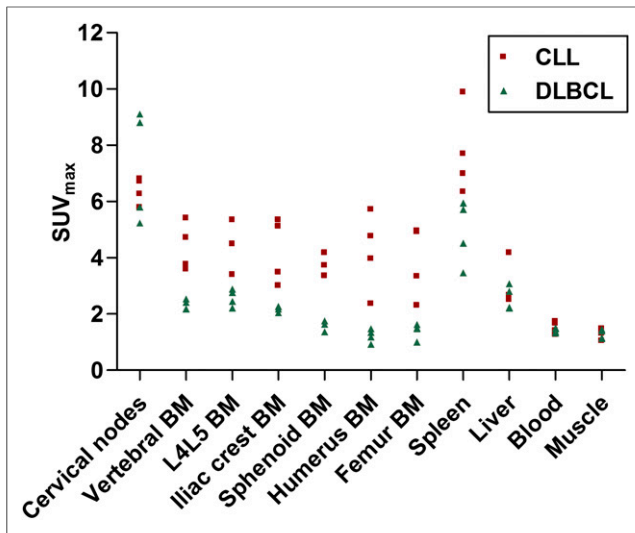
FIGURE 3. ^{18}F-fludarabine uptake in nodal sites, extranodal sites, and background regions for DLBCL and CLL patients. Data are SUV$_{max}$ (summed, 30–50 min; n = 4 per group). BM = bone marrow; L4L5 = lumbar vertebrae 4 and 5.

the purpose of measuring metabolic tumor volume on ^{18}F-fludarabine PET scans was to evaluate whether, through rapid clearance from normal tissues and retention in tumors, tumor-to-background contrast was high enough to make automatic segmentation of the involved sites feasible. Therefore, liver was used as the reference organ and was found to be a reproducible threshold for segmentation of involved sites in DLBCL patients (nodes) and CLL patients (nodes, bone marrow), on either early or late ^{18}F-fludarabine PET scans. Spleen was also segmented in both groups, although its involvement remains unconfirmed in DLBCL patients. To estimate the absorbed dose to critical organs, standard S values (MIRD method) were obtained with per-patient organ mass corrections. The mean effective dose for ^{18}F-fludarabine was below that reported for ^{18}F-FDG (*32*).

Although this pilot study was not without weaknesses—mainly the small population of patients—the DLBCL and CLL imaging studies with ^{18}F-fludarabine PET afforded several positive points. The images were already highly satisfactory at the early time point of 30–50 min after injection. The specificity of the probe for lymphoid cells, and absence of accumulation in inflammatory tissues, facilitated image interpretation. The ability of ^{18}F-fludarabine PET to detect indolent lymphoma and bone marrow infiltration may play a key role in determining the stage, treatment, and prognosis of lymphoma, for which ^{18}F-FDG PET is still controversial. Moreover, the radiation dose of ^{18}F-fludarabine is low. A prospective multicenter study (national grant PHRC-K 2016 from Programme Hospitalier de Recherche Clinique en Cancérologie) is in progress to determine the place of ^{18}F-fludarabine PET/CT in ^{18}F-FDG–avid lymphoma imaging. The capabilities of ^{18}F-fludarabine PET in the management of indolent non–Hodgkin lymphoma that is not ^{18}F-FDG–avid should also be assessed.

CONCLUSION

^{18}F-fludarabine PET/CT appears to be a promising tool for lymphoproliferative diseases. The radiation dose of this radiopharmaceutical is below that of ^{18}F-FDG. The specificity of this PET probe for lymphoid cells, its absence of accumulation in reactive tissues, and its feasibility for detection of bone marrow infiltration might play an innovative role in lymphoma imaging.

REFERENCES

1. Swerdlow SH, Campo E, Pileri SA, et al. The 2016 revision of the World Health Organization classification of lymphoid neoplasms. *Blood.* 2016;127: 2375–2390.
2. Kostakoglu L. Novel PET radiotracers for potential use in management of lymphoma. *PET Clin.* 2012;7:83–117.
3. Gallamini A, Zwarthoed C, Borra A. Positron Emission Tomography (PET) in oncology. *Cancers (Basel).* 2014;6:1821–1889.
4. André MPE, Girinsky T, Federico M, Reman O, Fortpied C, Gotti M. Early positron emission tomography response-adapted treatment in stage I and II Hodgkin lymphoma: final results of the randomized EORTC/LYSA/FIL H10 trial. *J Clin Oncol.* 2017;35:1786–1794.
5. Barrington SF, Mikhaeel NG. When should FDG-PET be used in the modern management of lymphoma? *Br J Haematol.* 2014;164:315–328.
6. Meignan M, Itti E, Gallamini A, Younes A. FDG PET/CT imaging as a biomarker in lymphoma. *Eur J Nucl Med Mol Imaging.* 2015;42:623–633.
7. Kostakoglu L, Cheson BD. State-of-the-art research on "lymphomas: role of molecular imaging for staging, prognostic evaluation, and treatment response." *Front Oncol.* 2013;3:212.
8. Kubota R, Yamada S, Kubota K, Ishiwata K, Tamahashi N, Ido T. Intratumoral distribution of fluorine-18-fluorodeoxyglucose in vivo: high accumulation in macrophages and granulation tissues studied by microautoradiography. *J Nucl Med.* 1992;33:1972–1980.
9. Kazama T, Faria SC, Varavithya V, Phongkitkarun S, Ito H, Macapinlac HA. FDG-PET in the evaluation of treatment for lymphoma: clinical usefulness and pitfalls. *Radiographics.* 2005;25:191–207.
10. Avivi I, Zilberlicht A, Dann JE, et al. Strikingly high false positivity of surveillance FDG-PET/CT scanning among patients with diffuse large cell lymphoma in the rituximab era. *Am J Hematol.* 2013;88:400–405.
11. Conte MJ, Bowen DA, Wiseman GA, et al. Use of positron emission tomography-computed tomography in the management of patients with chronic lymphocytic leukemia/small lymphocytic lymphoma. *Leuk Lymphoma.* 2014;55:2079–2084.
12. Wang X. PET/CT appropriate application in lymphoma. *Chin Clin Oncol.* 2015; 4:4.
13. Guillouet S, Patin D, Tirel O, et al. Fully automated radiosynthesis of 2-[^{18}F] fludarabine for PET imaging of low-grade lymphoma. *Mol Imaging Biol.* 2014; 16:28–35.
14. Gandhi V, Plunkett W. Cellular and clinical pharmacology of fludarabine. *Clin Pharmacokinet.* 2002;41:93–103.
15. Montillo M, Ricci F, Tedeschi A. Role of fludarabine in hematological malignancies. *Expert Rev Anticancer Ther.* 2006;6:1141–1161.
16. Lenz G, Hiddemann W, Dreyling M. The role of fludarabine in the treatment of follicular and mantle cell lymphoma. *Cancer.* 2004;101:883–893.
17. Cividini F, Pesi R, Chaloin L, et al. The purine analog fludarabine acts as a cytosolic 5′-nucleotidase II inhibitor. *Biochem Pharmacol.* 2015;94:63–68.
18. Dhilly M, Guillouet S, Patin D, et al. 2-[^{18}F]fludarabine, a novel positron emission tomography (PET) tracer for imaging lymphoma: a micro-PET study in murine models. *Mol Imaging Biol.* 2014;16:118–126.

19. Hovhannisyan N, Guillouet S, Fillesoye F, et al. Evaluation of the specificity of [18F]fludarabine PET/CT in a xenograft model of follicular lymphoma: comparison with [18F]FDG and impact of rituximab therapy. *EJNMMI Res.* 2015;5:23.

20. Hovhannisyan N, Dhilly M, Guillouet S, Leporrier M, Barré L. Comparative analysis between [18F]fludarabine-PET and [18F]FDG-PET in a murine model of inflammation. *Mol Pharm.* 2016;13:2136–2139.

21. Grégoire V, Van NT, Stephens LC, et al. The role of fludarabine-induced apoptosis and cell cycle synchronization in enhanced murine tumor radiation response in vivo. *Cancer Res.* 1994;54:6201–6209.

22. Hallek M, Catovsky D, Caligaris-Cappio F, et al. Guidelines for the diagnosis and treatment of chronic lymphocytic leukemia: a report from the International Workshop on Chronic Lymphocytic Leukemia updating the National Cancer Institute-Working Group 1996 guidelines. *Blood.* 2008;111:5446–5456.

23. Campo E, Swerdlow SH, Harris NL, Pileri S, Stein H, Jaffe ES. The 2008 WHO classification of lymphoid neoplasms and beyond: evolving concepts and practical applications. *Blood.* 2011;117:5019–5032.

24. Wahl RL, Jacene H, Kasamon Y, Lodge MA. From RECIST to PERCIST: evolving considerations for PET response criteria in solid tumors. *J Nucl Med.* 2009;50(suppl):122S–150S.

25. Cheson BD, Fisher RI, Barrington SF, et al. Recommendations for initial evaluation, staging, and response assessment of Hodgkin and non-Hodgkin lymphoma: the Lugano classification. *J Clin Oncol.* 2014;32:3059–3068.

26. Siegel JA, Thomas SR, Stubbs JB, et al. MIRD pamphlet no. 16: techniques for quantitative radiopharmaceutical biodistribution data acquisition and analysis for use in human radiation dose estimates. *J Nucl Med.* 1999;40(suppl):37S–61S.

27. Adams HJ, Kwee TC. Proportion of false-positive lesions at interim and end-of-treatment FDG-PET in lymphoma as determined by histology: systematic review and meta-analysis. *Eur J Radiol.* 2016;85:1963–1970.

28. Rayamajhi SJ, Mittal BR, Maturu VN, et al. 18F-FDG and 18F-FLT PET/CT imaging in the characterization of mediastinal lymph nodes. *Ann Nucl Med.* 2016;30:207–216.

29. Cheng CY, Mruk DD. The blood-testis barrier and its implications for male contraception. *Pharmacol Rev.* 2012;64:16–64.

30. Zhu D, Ma T, Niu Z, et al. Prognostic significance of metabolic parameters measured by 18F-fluorodeoxyglucose positron emission tomography/computed tomography in patients with small cell lung cancer. *Lung Cancer.* 2011;73:332–337.

31. Yang DH, Ahn JS, Byun BH, et al. Interim PET/CT-based prognostic model for the treatment of diffuse large B cell lymphoma in the post-rituximab era. *Ann Hematol.* 2013;92:471–479.

32. Willowson KP, Bailey EA, Bailey DL. A retrospective evaluation of radiation dose associated with low dose FDG protocols in whole-body PET/CT. *Australas Phys Eng Sci Med.* 2012;35:49–53.